Effects of Additives on Kinetics, Morphologies and Lead-Sensing Property of Electrodeposited Bismuth Films

Journal:	*The Journal of Physical Chemistry*
Manuscript ID	jp-2016-06924u.R1
Manuscript Type:	Article
Date Submitted by the Author:	05-Sep-2016
Complete List of Authors:	Rajamani, Athimotlu Raju ; Amrita Vishwa Vidyapeetham; Amrita Vishwa Vidyapeetham Jothi, Sathiskumar; Swansea University Kumar, Murugaiah Dhinesh; Amrita Vishwa Vidyapeetham Srinivasan, Srikaanth; Amrita Vishwa Vidyapeetham Singh, Manoj; Departamento de Engenharia Mecanica, Centre for Mechanical Technology Otero Irurueta, Gonzalo; Universidade de Aveiro, Center for Mechanical Technology and ... Ramasamy, Devaraj; Centre of Mechanical Technology and Automation, Department of Mechanical Engineering Datta, Madhav; Amrita Vishwa Vidyapeetham; Amrita Vishwa Vidyapeetham Rangarajan, Murali; Amrita Vishwa Vidyapeetham University; Amrita Vishwa Vidyapeetham

Effects of Additives on Kinetics, Morphologies and Lead-Sensing Property of Electrodeposited Bismuth Films

Athimotlu Raju Rajamani,[1,2] Sathiskumar Jothi,[3] Murugaiah Dhinesh Kumar,[2] Srinivasan Srikaanth,[2] Manoj Kumar Singh,[4] Gonzalo Otero-Irurueta,[4] Devaraj Ramasamy,[4] Madhav Datta,[1,5] Murali Rangarajan[1,2]*

[1]Center of Excellence in Advanced Materials and Green Technologies, Amrita School of Engineering Coimbatore, Amrita Vishwa Vidyapeetham, Amrita University, India

[2]Department of Chemical Engineering and Materials Science, Amrita School of Engineering Coimbatore, Amrita Vishwa Vidyapeetham, Amrita University, India

[3]Material Research Centre, College of Engineering, Swansea University, Bay Campus, Fabian Way, Swansea SA1 8EN, UK

[4]Centre for Mechanical Technology & Automation, Department of Mechanical Engineering, University of Aveiro, 3810-193 Aveiro, Portugal

[5]Amrita Center for Industrial Research and Innovation, Amrita School of Engineering Coimbatore, Amrita Vishwa Vidyapeetham, Amrita University, India

ABSTRACT

This study presents a systematic examination of the effects of bath additives and deposition conditions on the rates of electrodeposition of bismuth, obtained morphologies, and the ability of the bismuth films to detect trace concentrations of lead. Novel morphologies of bismuth are reported for the first time. The bath comprises bismuth nitrate, nitric acid, and a set of additives, viz., citric acid (complexant), polyvinyl alcohol (surface inhibitor), and betaine (grain refiner). Rotating disk electrode voltammetry and cyclic voltammetry have been used to determine the mechanism and rates of bismuth electrodeposition. Scanning electron microscopy is used to study deposit morphologies, while X-ray diffraction and X-ray photoelectron spectroscopy have been used to examine crystallinity and composition of the deposited thin films. Even in the presence of additives, it is seen that bismuth deposition is diffusion-controlled process with progressive nucleation-growth of crystallites, and the reduction is a single-step, three-electron-transfer, quasi-reversible reaction. The films deposited from the bath without additives comprise micron-sized, hexagonal rods with controlled aspect ratios (1.83 to 2.05). Baths containing citric acid produce films with flower-like structures and cracked grains, but with poor adhesion to copper substrate. Introducing polyvinyl alcohol significantly slows down bismuth deposition, increases the number of nuclei, produces cauliflower-like crystallites, and promotes adhesion to copper. Betaine smoothens these crystallites while retaining good adhesion. Pulsing the deposition current promotes growth of existing nuclei. In the absence of additives, fused flat disk-type spindles are seen. In the presence of additives, pulsed deposition results in sea-urchin-like morphologies. Adhesion of bismuth onto copper impacts the ability of the film to detect trace concentration of Pb^{2+} ions in aqueous solutions using anodic stripping voltammetry. The

films obtained from baths with additives through direct current plating show the best sensor response for 50 ppb Pb^{2+}.

INTRODUCTION

Electrodeposition of metal thin films have been studied extensively for a wide range of applications from decorative finishing to enhancements in mechanical, electrical, and catalytic properties. It is well known that introducing additives in the bath alter the rate of electrodeposition and possibly the mechanism, thereby resulting in qualitatively different surface morphologies, adhesion, and properties of interest.[1] In this work, the effects of bath additives and process conditions on electrodeposition of bismuth are examined systematically.

Bismuth thin films have evinced significant interest recently owing to a number of its attractive properties such as highly anisotropic Fermi surface, Dirac valley degeneracy,[2] small energy overlap between its valence and conduction bands, small effective charge carrier mass, long charge carrier mean-free path.[3] By introducing a semi-metal to semiconductor transition, it has been possible to enhance Seebeck coefficient of bismuth films, thereby making it an attractive thermoelectric material.[4] Owing to its long charge carrier mean-free paths, bismuth has shown excellent magnetoresistance (150-350%) even at room temperature.[5,6] Bismuth has also shown promising electrochromic behavior for black on white/yellow, arising from its quasi-reversible deposition-dissolution.[7] Perhaps the most studied application of bismuth is in electrochemical sensing of a variety of analytes, particularly heavy metals.[8] This arises from the ease with which bismuth forms solid solutions and alloys with most metals, similar to mercury. However, bismuth is considerably less toxic and therefore has attracted more interest.

Bismuth films have been synthesized by a number of processes, viz., thermal evaporation, sputtering, laser deposition, sol-gel method, and electrodeposition.[9-18] Various morphologies

have been obtained such as hexagons, rhombohedrons, wires, spheres, tubes, triangles, belts, and dendrites. Among the different techniques to prepare bismuth thin films, electrodeposition has unique advantages of simplicity, speed, and ease of control. The mechanisms of bismuth electrodeposition from different baths have been studied,[19] with nitrate being the most commonly used bath. It is known that bismuth deposition is a quasi-reversible, single-step, three-electron-transfer reduction that is diffusion-controlled.[17,20] There is evidence of underpotential deposition of bismuth on certain electrodes,[21] and it has been observed that new bismuth crystallites nucleate on growing crystallites and grow in a progressive nucleation-and-growth fashion.[17,20] However, the effects of bath additives on bismuth electrodeposition, specifically on the reduction kinetics and on the obtained morphologies, have not been explored. This work considers three additives – a complexant (citric acid), a surface inhibitor (polyvinyl alcohol) and a grain refiner (betaine) – in an acidic nitrate bath. Citric acid has long been used in electrodeposition of metals and alloys for its ability to complex metal ions as citrates thereby influencing reduction kinetics.[22-27] Polyvinyl alcohol is chosen as an additive because of its known ability to improve adhesion of films, facilitate uniform film formation, increase of nuclei density, reduction of grain size, and because of its green and non-toxic nature.[28,29] It is seen that the introduction of these additives improves the adhesion of the deposits and significantly enhances the response of the electrodeposited films in ultratrace detection of heavy metals such as lead.

EXPERIMENTAL SECTION

Throughout the study, chemicals of analytical grade were used, and solutions were prepared using ultrapure water (18 MΩ, MilliQ, Millipore). Electroanalytical experiments – cyclic voltammetry, rotating disk voltammetry, bulk electrolysis and square wave anodic voltammetry – were carried out using the WaveNow potentiostat and the rotating disc electrode facility of

Pine Instruments, Inc. A three-electrode system was used, with polycrystalline copper sheet as working electrode, platinum wire as counter electrode and Ag/AgCl as reference electrode. For bulk electrolysis, a polycrystalline copper cathode (1×2 cm^2) with stainless steel anodes kept parallel on either side was used. Prior to experiments, the copper foil was cleaned in acetic acid for five minutes, followed by ultrasonication in acetone and in ultrapure water for two minutes each, to remove oxide layers present. Morphology analysis was carried out using a FEI Quanta FEG 200 scanning electron microscope. Powder X-ray diffraction (XRD) studies were conducted on X'pert PRO of PANalytical diffractometer with Cu-Kα X-rays of wavelength (λ) 1.54056 A°. X-ray photoelectron spectroscopy (XPS) studies were carried out in an Ultra High Vacuum (UHV) system with a base pressure of 1×10^{-10} mbar. The system is equipped with a hemispherical electron energy analyzer (SPECS Phoibos 150), a delay-line detector and a monochromatic Al Kα (1486.74 eV) X-ray source. High resolution spectra were recorded at normal emission take-off angle and with a pass-energy of 20 eV, which provides an overall instrumental peak broadening of 0.5 eV.

RESULTS AND DISCUSSION

Voltammetric Studies of Bismuth Deposition: The effects of bath additives on bismuth deposition have been examined by using cyclic voltammetry (CV) and linear sweep voltammetry on a rotating disk electrode (LSV-RDE). The additives considered for this study include a complexant (citric acid, CA, 0.1 or 0.2 M), surface inhibitor (polyvinyl alcohol, PVA, 5 grams per liter, *gpl*), and a grain refiner (betaine, BET, 0.01 M). Their structures are given in Figure S1(a-c). Linear sweep voltammograms on rotating disk electrode shows limiting currents for all four systems studied (Figure 1a and Figures S2a-c). It is of interest to note that introducing additives does not change the rate-limiting step of the process, which remains diffusion. The

decreased slopes of the results fitted to Levich equation indicate that the diffusion coefficient of bismuth ions further decreases with the introduction of additives. LSV-RDE results, shown in Figure 1a, confirm that the deposition is diffusion-controlled, as evidenced from the limiting currents that increase with the rate of rotation of the electrode according to the Levich equation (Figure 1b)

$$I_l = (0.201)nFAD^{2/3}\omega^{1/2}\nu^{-1/6}C_O, \qquad (1)$$

where n is the number of electrons transferred in the reduction reaction (n = 3), F is Faraday's constant (96487 C/mol), A is the area of the electrode, D is the diffusion coefficient of the bismuth ion, ω is the speed of rotation of the electrode (in rotation per minute, rpm), ν is the kinematic viscosity of the solution (cm^2/s), and C_O is the bulk concentration of bismuth ion (mol/cm^3).[30]

The cyclic voltammogram in Figure 2a shows that the Bi^{3+} reduction on copper electrode is a single-step, quasi-reversible, three-electron transfer reaction. This has been confirmed in our previous study and other earlier reports.[17,20] In the present work, it is seen that the introduction of additives does not alter this mechanism. The nucleation process has been found to be closer to progressive nucleation-growth model.[31] It is known that, at higher scan rates, a quasi-reversible redox reaction shows irreversible behavior. Cyclic voltammograms have been obtained (Figure S3a-d) at different scan rates for the four systems corresponding to those in Figure 2. For a diffusion-limited, irreversible reaction,

$$Bi^{3+} + 3e \xrightarrow{k_f} Bi \qquad (2)$$

the surface concentration of bismuth ions is determined by matching the diffusion flux to the flux of three-electron-transfer reduction, given by

$$\frac{i}{nFA} = D\left[\frac{\partial C_{Bi3+}(x,t)}{\partial x}\right]_{x=0} = k_f C_{Bi3+}(0,t), \forall t. \qquad (3)$$

Bard and Faulkner[30] give the current functions for irreversible charge transfer at an electrode. From the maximum of the current function, an expression for the peak current may be obtained as a function of bismuth ion concentration in the bulk solution as

$$i_p = 0.227nFAC_O{}^* k_f = 0.227nFAC_O{}^* k_0 \exp\left[-\frac{\alpha nF}{RT}\left(E_p - E_0'\right)\right], \qquad (4)$$

where n is the number of electrons transferred, F is Faraday's constant, A is the electroactive surface area, $C_O{}^*$ is the concentration of bismuth ions in the solution, k_0 is the effective heterogeneous standard rate constant, α is the transfer coefficient, E_p is the peak potential and E_0' is the formal potential. The effective heterogeneous rate constant for bismuth ion reduction, k_0, may then simply be obtained from the intercept of a plot of *ln* i_p and ($E_p - E_0$'). The shapes of the cyclic voltammograms indicate that electron transfer during bismuth deposition occurs in a single step even in the presence of additives. Thus, electroreduction of Bi^{3+} from different baths containing additives (see Table 1 for the four different samples A-D studied here) at scan rates ≥ 100 mV/s has been modeled as an equivalent one-step, three-electron-transfer, irreversible process. The magnitude of the effective heterogeneous rate constant then provides an estimate of the net rate of bismuth electrodeposition.

The reduction peak potential and current density for bismuth in the absence of additives are, respectively, – 34.7 mV and – 7.4 mA/cm^2, while the effective heterogeneous rate constant is estimated to be 0.0504 cm/s. Introduction of citric acid shifts the reduction potential further cathodically to – 54.7 mV and does not change the peak current density significantly (– 7.5 mA/cm^2), while k_0 is found to be 0.0337 cm/s. It is seen that additional overpotential is needed to reduce the bismuth ions. Also, the effective rate constant is significantly reduced, indicating that

the reduction is slowed down. However, at lower scan rates, this does not seem clear, as the peak current density does not show a significant variation. The slower rate of reduction is masked by the increased number of nucleation sites, as seen in the SEM images (Figure S5a, compared to Figure 3b), thereby resulting in a higher peak current. At fast scan rates, progressive nucleation-growth is further retarded, resulting in smaller peak current densities. We believe that the slower reduction of bismuth is due to the formation of bismuth citrate in solution. Citric acid is known to complex bismuth,[32] in solution to form various bismuth citrate complexes. The complex is also known to polymerize through carboxylate bridges. However, at low solution pH (due to the supporting electrolyte 0.4 M HNO_3), the most likely compound to be present is the simple citrate $BiC_6H_5O_7$, and even so, it is unlikely that all bismuth ions are present as citrate. The citrate likely exists in an equilibrium with bismuth ions in the solution, with the equilibrium being shifted to the release of the bismuth ions due to the electroreduction followed by growth of bismuth crystallites. There is no evidence of significant adsorption of citrate/complex onto the electrode surface, as seen by the shape of the voltammogram. Thus, the increased overpotential needed for bismuth reduction is likely associated with the dissociation of bismuth citrate and the formation of more nuclei on the electrode surface. At this juncture, it is important to note that as bismuth deposits and the crystallites grow, the electroactive surface area of the electrode changes dynamically, which has not been accounted for explicitly. Thus, these heterogeneous rate constants capture a more complex behavior, including, in this instance, the rate of the preceding reversible dissociation reaction of bismuth citrate, the increased number of nuclei available as crystals grow, and the increase in electroactive surface area due to progressive nucleation.

Introducing polyvinyl alcohol (PVA) further cathodically shifts the reduction potential to – 84.2 mV and reduces the peak current density to – 5.8 mA/cm^2, and the rate constant to 0.0122 cm/s.

Polymers such as polyethylene glycol (PEG), polyethylene imine (PEI), and PVA have been used for adsorption at a copper electrode.[33,34] Adsorption of PVA would partially block active nucleation sites on copper for bismuth crystal growth thereby requiring higher overpotential and slowing the rate of bismuth reduction. This is reflected by both a nearly 23% decrease in the peak current density as well as a significantly smaller rate constant. Quantitatively, the rate constant is about 24% of that without additives. However, the current density observed is much higher, due to the significantly increased number of nuclei (as evidenced in Figure 3f) and the consequent increase in electroactive surface area. Introducing a grain refiner betaine in the bath does not alter the reduction potential of bismuth, – 84.3 mV, but improves the peak current density to – 6.5 mA/cm^2, and the effective rate constant is reduced to 0.01067 cm/s. Though betaine appears to further slow the reduction, as a grain refiner, it provides additional nucleation sites for bismuth crystal growth, thereby increasing the current density.

Deposit Morphologies: Electrodeposition of bismuth has been carried out by passing either a constant current or a pulsed current. The morphologies of electrodeposited bismuth under different conditions have been examined by high resolution scanning electron microscopy (HR-SEM). In all, six different samples have been analyzed, as given in Table 1. These capture the effects of current density, bismuth concentration, additives, and of pulsing the current. In all the samples, there is clear evidence of bismuth growing in a progressive nucleation-and-growth fashion. The base set of bath and deposition parameters are 10 mM Bi^{3+} and 0.4 M HNO_3, with deposition at a constant current density of 10 mA/cm^2 (Sample A). Under these conditions, micron-sized bismuth hexagonal rods and high surface roughness are formed onto copper substrate (Figure 3a-b). However, the deposit does not adhere well with the substrate, as seen in Figure S4(A).

The introduction of the surfactant citric acid introduces a profound change in the morphology of electrodeposited bismuth (Sample B). It is seen that nucleation of bismuth starts at specific locations on the electrode surface and growth takes place outward in flower-like shapes (Figure 3c-d). The intermediate regions are filled with fine-grained structures that have cracks. Increasing the citric acid concentration results in pronounced cracks, with layered foliage-like morphology (Figure S5a-d). There are regions with large number of nuclei, both on copper surface and on the growing bismuth crystallites. Due to high density of nuclei yet and slow rates of deposition/growth, many of the crystallites are unable to grow into large structures like the hexagonal rods seen in Figure 3a. Even the introduction of citric acid does not significantly improve adhesion of the deposit onto copper (Figure S4(B)). The addition of polyvinyl alcohol along with citric acid clearly facilitates nucleation of bismuth crystallites on copper surface, promotes strong adhesion between bismuth and copper, and eliminates cracks, resulting in fine grains of bismuth with excellent surface coverage (Sample C, Figures 3e-f, S4(C)). Finer cauliflower-like morphologies are obtained under conditions of slow deposition with progressive nucleation. Introducing betaine further refines the grain size but yields similar morphologies with good adhesion (Sample D, Figures 3g-h, S4(D)).

When the plating current is pulsed (10 mA/cm^2 peak current density and a 10 ms:10 ms on:off duration pulse) for deposition from an additive-free bath, spindle-like morphologies are obtained (Sample E). The time during which no current flows allows for the reduced bismuth adatoms to grow on to existing nuclei, resulting in longer, flat disk-shaped morphologies that attach with each other to form spindles. Thus, each spindle consists of a set of disks which have nucleated together (Figure 4a-b). Introduction of bath additives significantly alters the morphology (Sample F). Pulsing the current significantly reduces the number of nuclei on copper substrate,

rather favoring the formation of nuclei on existing crystallites. Combined with slower reduction rates as seen in the voltammetric studies, the surface coverage is reduced significantly in Sample F compared to Sample D, where bismuth is deposited from the same bath with a direct current density of 10 mA/cm^2. The resultant morphology resembles a sea urchin like structure (Figure 4c-d). It is to be noted that the peak current density for pulsed current deposition has been held at 10 mA/cm^2, therefore the average current density is 5 mA/cm^2. This reduction in the average current density also would have contributed significantly to the reduced surface coverage.

Deposit Crystallinity and Composition*:* Figures 5 and 6 show the X-ray diffraction patterns and X-ray photoelectron spectra, respectively, of the six electrodeposited bismuth samples. It is found that all the films are crystalline in nature. In addition to peaks corresponding to bismuth, samples A (no additives) and B (with citric acid) also show a peak at 24.5°, corresponding to the (1 0 1) plane of bismuth oxide (JCPDS). In fact, the XPS spectra for all the six samples show the presence of bismuth oxide (159.0 eV, Bi4f$_{7/2}$ and 164.5 eV, Bi4f$_{5/2}$) which is the result of surface oxidation. However, samples A and B do not show a prominent bismuth peak (Figure 6A and 6B). The remaining samples show clear peaks at binding energies 157.0 eV (Bi4f$_{7/2}$) and 162.5 eV (Bi4f$_{5/2}$), corresponding to bismuth. In the six samples (Table 1), there are clear crystalline peaks corresponding to polycrystalline bismuth (JCPDS: 85-1329). The adhesion of bismuth onto copper substrate is very poor for dc plating in the absence of additives and in the presence of citric acid alone as the bath additive. On the other hand, introduction of PVA significantly enhances adhesion, and this likely prevents significant oxidation of the electrodeposited bismuth to bismuth oxide. Similarly, pulsing the current also improves adhesion between copper and bismuth, as reported for other electrodeposition systems.[35] Pulsed current possibly helps in minimizing the oxidation of electrodeposited bismuth films.

The preferred orientations of all the six electrodeposited films are (0 1 2), (1 0 4), (1 1 0) planes. Pulsing the current does not significantly alter the diffraction patterns. The intensity and the extent of broadening of diffraction peaks are different for the different samples, indicating variations of crystalline size and lattice strain in the presence of additives. The average crystallite size of the bismuth may be calculated using the Scherrer formula

$$D = \frac{k\lambda}{\beta \cos\theta}, \qquad (5)$$

where k is a constant (0.94), λ is the wavelength of X-ray (1.5406Å), β is the full-width-half-maxima (FWHM) of the peak, and θ is the Bragg's angle, 27.15°, corresponding to the (0 1 2) plane. The obtained crystallites vary in size from 30 to 45 nm. In the absence of additives, the crystallite size is 30.2 nm, which increases to 45.0 nm in the presence of citric acid. This is consistent with the slower bismuth reduction, which allows for larger crystallite sizes. As the addition of PVA and betaine promotes nucleation while further slowing effective rate of reduction, this results in smaller crystallites, though better surface coverage. Thus, the crystallite sizes for samples C and D are 38.2 and 37.4 nm, respectively. When the current is pulsed, slower growth rates and more time for the reduced bismuth atoms to grow on existing nuclei imply that the crystallite size (37.1 nm) is larger than those from deposition with direct current (30.2 nm). Introduction of additives with pulsed current deposition further slows down the deposition and results in smaller crystallite size (34.5 nm).

Wide-scan X-ray photoelectron spectra are available in Figure S6a. It is seen that there are peaks for carbon as well as oxygen, with a nitrogen peak for Samples A and B. Mostly these appear to be surface contaminants.[36] The spectra for carbon, oxygen, and nitrogen are shown in Figures S6b-d. The primary carbon peak is for C=C (sp^2 carbon with binding energy of 284.8 to 285 eV), while the remaining peaks for C–O (hydroxyl with binding energy of 286.6 eV) and

C(=O)–O (carboxyl with binding energy of 288.8 eV). Though these peaks are present in all the six samples, the percentage of hydroxyl and carboxyl carbon groups are higher in the samples containing additives plated with direct current, particularly with PVA and betaine (Samples C and D). On the one hand, these results imply that small quantities of citrate and PVA are adsorbed on the surface. Given the significant difference in their amounts added to the solution (19.2 gpl citric acid vs. 5 gpl PVA), it may be stated that PVA adsorbs more strongly onto the depositing film than citrate. On the other hand, cyclic voltammograms do not show any signatures of adsorptive kinetics, indicating that the adsorbed citrate does not significantly alter the mechanism or kinetics of deposition. The adsorbed citrate and PVA, however, provide additional nucleation sites for bismuth crystallites to grow.

Heavy Metal Sensing: One of the most well-studied applications of electrodeposited bismuth thin films is their ability to detect trace quantities of heavy metals because of bismuth's unique ability to form solid solutions with most metals.[37,38] The preferred technique for bismuth-based electrochemical sensing of heavy metals is anodic stripping voltammetry – square wave or differential pulse – with a cathodic preconcentration step,[39,40] due to increased sensitivity. To examine the influence of bismuth morphology on heavy metal sensing, detection of lead has been attempted. A standard solution of 50 ppb of Pb^{2+} ion has been chosen, and square wave anodic stripping voltammetry has been used to detect lead. One of the challenges with electrodeposited bismuth films on copper is poor adhesion, which has been overcome in this work with the use of additives. Following a cathodic preconcentration at – 0.7 V for 600 seconds, the anodic stripping potential has been swept from – 0.7 to – 0.3 V. Lead is stripped at ~ – 0.55 V. The results are presented in Figure 7. Samples A and B are unable to detect lead at 50 ppb, owing to their poor adhesion on copper substrate. Sample D, with all three additives,

shows maximum peak current, followed by Sample C, with citric acid and polyvinyl alcohol. The films deposited with pulsed current show lower peak currents than those with direct current. Sample F, with additives, gives stronger signal for 50 ppb lead than Sample E, without additives. Thus, it is clear that samples with good adhesion, large number of nuclei, and therefore larger electroactive surface area give maximum sensor response.

CONCLUSIONS

Electrodeposition of bismuth has been studied from acidic nitrate baths and confirmed to be diffusion-limited, single-step, quasireversible three-electron-transfer reduction process using RDE and cyclic voltammetry. Micron-sized hexagonal rods of bismuth are obtained from an acidic bath containing 10 mM Bi^{3+} and 0.4 M nitric acid. The effects of bath additives on the deposition mechanism, rates, morphologies, and the ability of bismuth deposits to detect trace concentration of lead have been examined. Even in the presence of additives, bismuth reduction is seen to be a single-step, three-electron-transfer process. Effective heterogeneous rate constants have been estimated from cyclic voltammograms measured at high scan rates ($\geq$ 100 mV/s) by treating the quasi-reversible reduction reaction (at high scan rates) as an equivalent one-step, irreversible process. Citric acid forms bismuth citrate in solution, slows deposition due to the additional reversible step of release of bismuth ions, increases the number of nuclei on the surface. The effective rate constant is reduced by a third though the peak current density at 50 mV/s scan rate is unaltered. Citric acid, however, does not enhance adhesion of the deposit onto the surface. Addition of polyvinyl alcohol slows down bismuth reduction further (effective rate constant is reduced by ~ 75%) by sterically blocking active sites on copper. However, it significantly promotes nucleation of new bismuth crystallites, and forms fine, micron-sized, cauliflower-like structures of bismuth with smaller sub-micron-sized modules. These structures

adhere well on copper, form a smooth film with homogeneous surface coverage. Betaine further smoothens and refines the crystallites, while resulting in similar morphologies. The obtained films are crystalline with some surface oxidation of bismuth to bismuth oxide, as revealed by XPS spectra. There is evidence of adsorption of citrate and polyvinyl alcohol on the surface and they are incorporated into the deposits. These provide additional nucleation sites for bismuth crystallites to grow. It is seen that bismuth films deposited from additive-containing baths (citric acid, PVA and betaine) give stronger response to 50 ppb Pb^{2+} ion by square wave anodic stripping voltammetry.

FIGURES

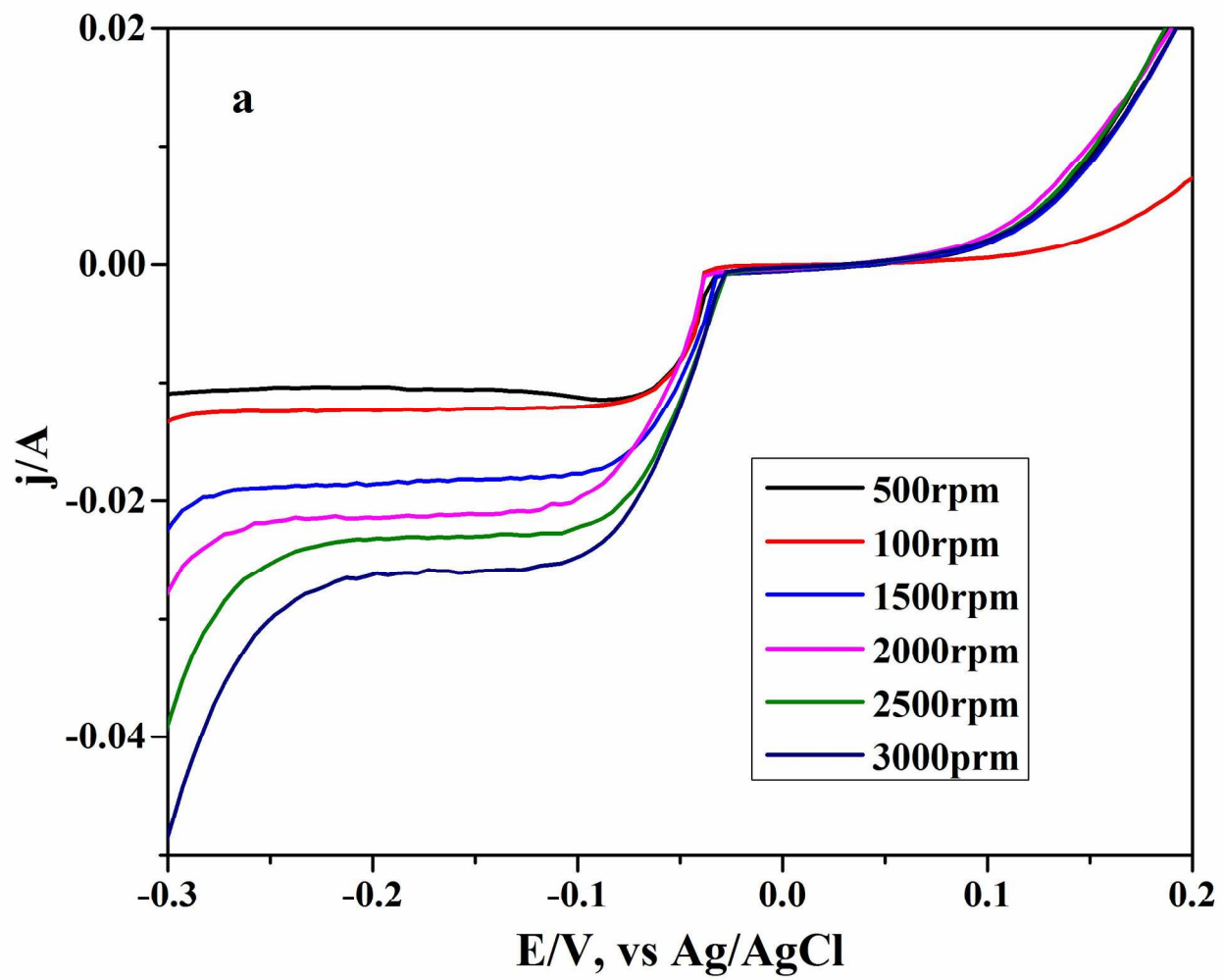
a
0.02
0.00
-0.02
-0.04
j/A
-0.3
-0.2
-0.1
0.0
0.1
0.2
E/V, vs Ag/AgCl
500rpm
100rpm
1500rpm
2000rpm
2500rpm
3000prm

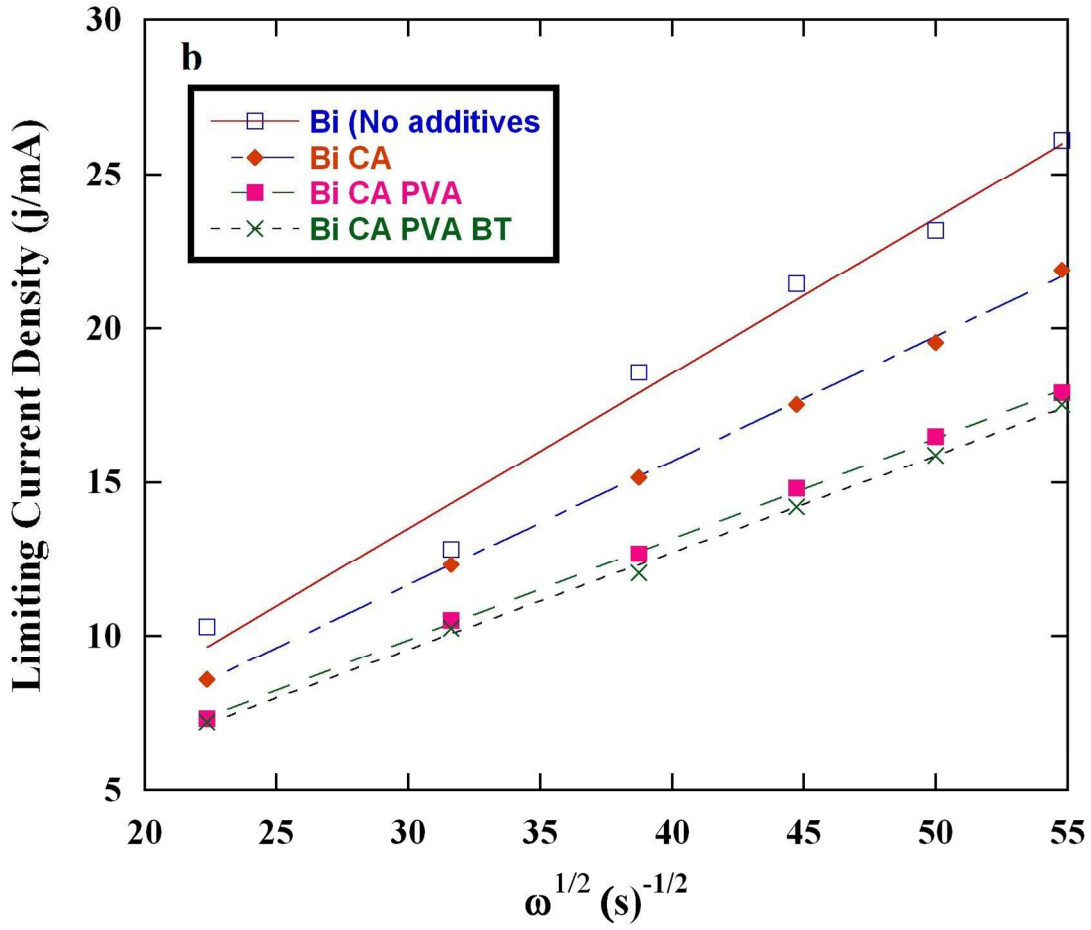

Figure 1a Rotating disk voltammetry study of bismuth deposition from a bath containing 0.01 M $Bi(NO_3)_3$ and 0.4 M HNO_3; **Figure 1b** Variation of limiting current as a function of square root of speed of rotation of the electrode, including the effects of additives: (□) – with no additives (slope = 0.504), (♦) – with 0.1 M citric acid (slope = 0.490), (■) – with 0.1 M citric acid and 5 gpl polyvinyl alcohol (slope = 0.327), (×) – with 0.1 M citric acid, 5 gpl polyvinyl alcohol and 0.01 M betaine (slope = 0.315)

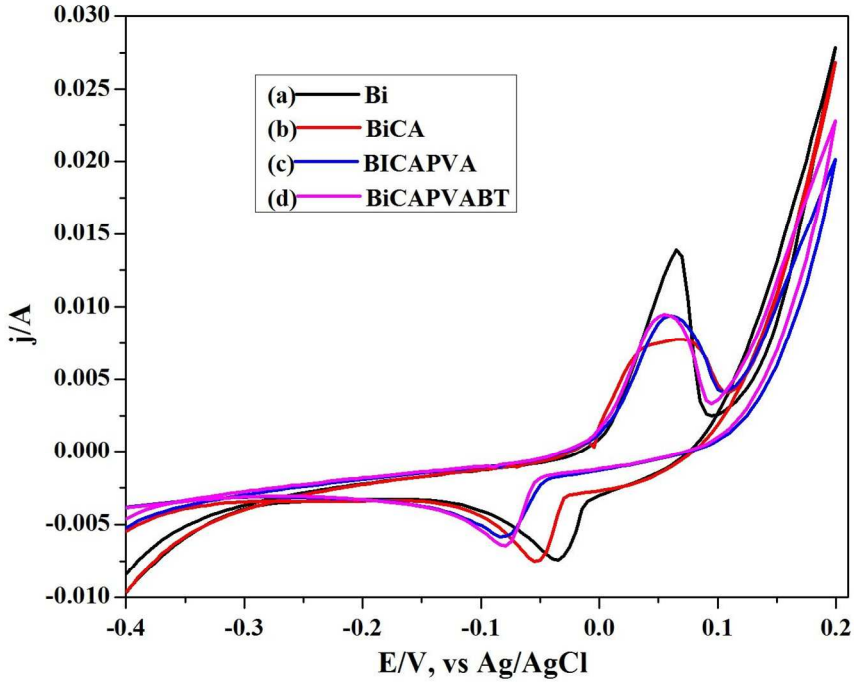

Figure 2. Cyclic voltammetry of Bi^{3+} reduction in baths containing 0.01 M $Bi(NO_3)_3$ and 0.4 M HNO_3; **(a)** No bath additives; **(b)** with 0.1 M citric acid; **(c)** with 0.1 M citric acid and 5 gpl polyvinyl alcohol; **(d)** with 0.1 M citric acid, 5 gpl polyvinyl alcohol and 0.01 M betaine at scan rate 50 mV/s

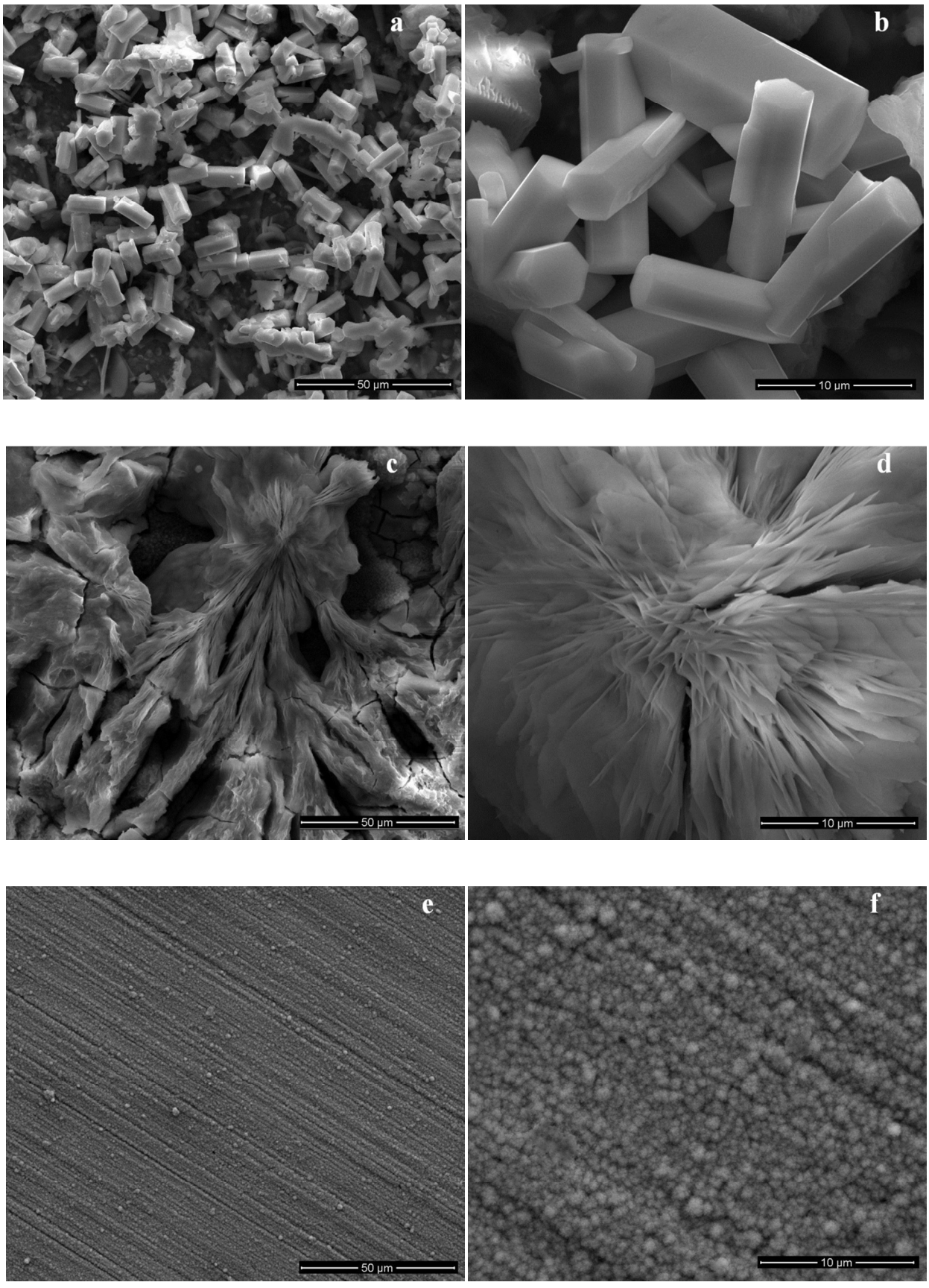
a
50 µm
b
10 µm
c
50 µm
d
10 µm
e
50 µm
f
10 µm

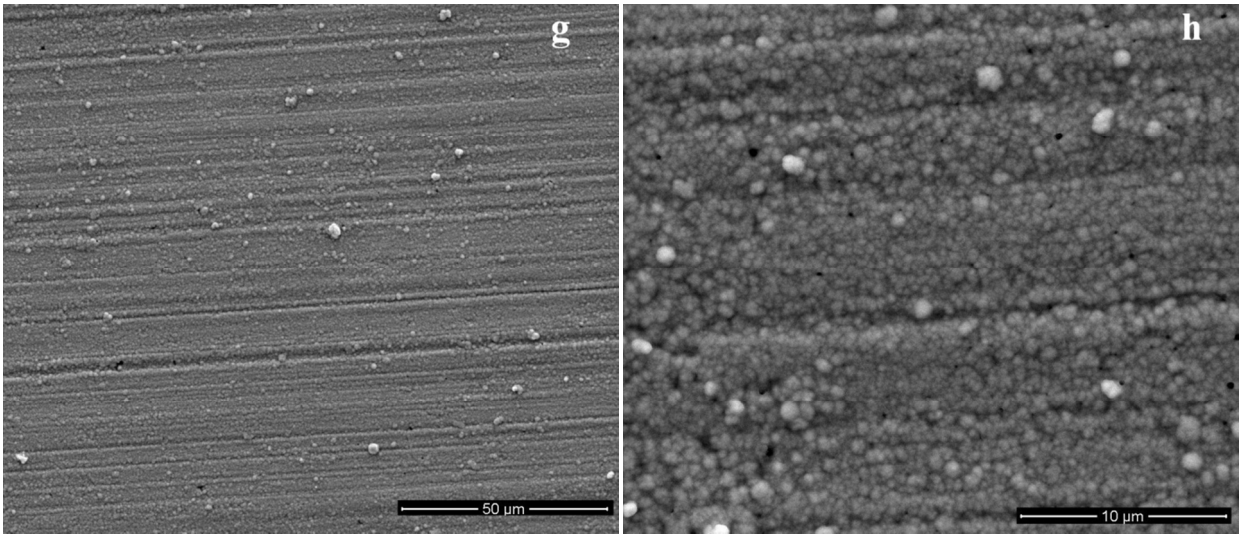

Figure 3. Scanning electron microscopy images of electrodeposited bismuth showing the effects of bath additives – for sample details, please see Table 1; **(a)** and **(b)** Sample A; **(c)**, and **(d)**, Sample B; **(e)** and **(f)** Sample C; **(g)** and **(h)** Sample D

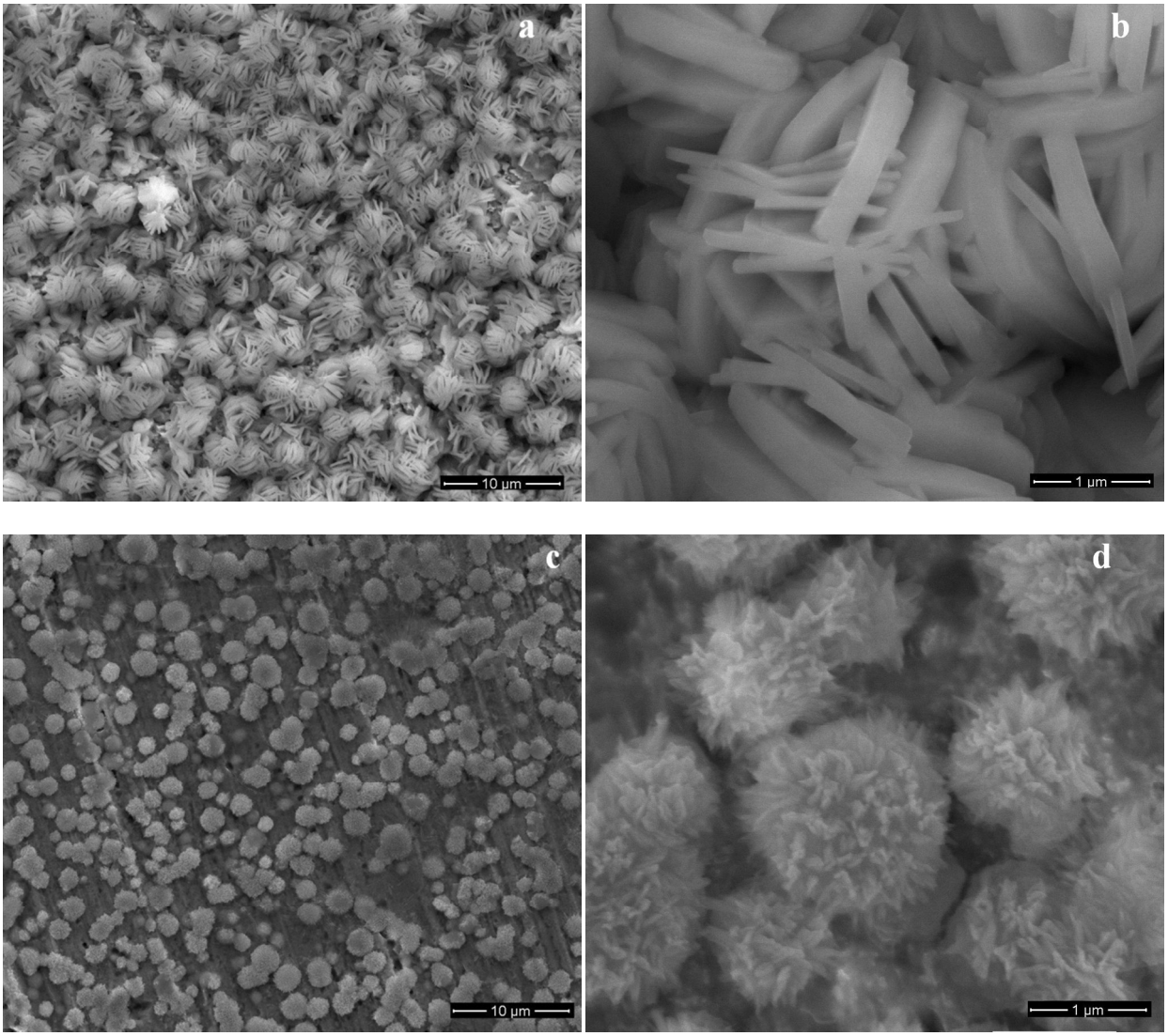

Figure 4. Scanning electron microscopy images of electrodeposited bismuth showing the effects of pulsing the current passed - for sample details, please see Table 1; **(a)** and **(b)** Sample E - spindle; **(c)** and **(d)** Sample F - sea urchin-like morphology

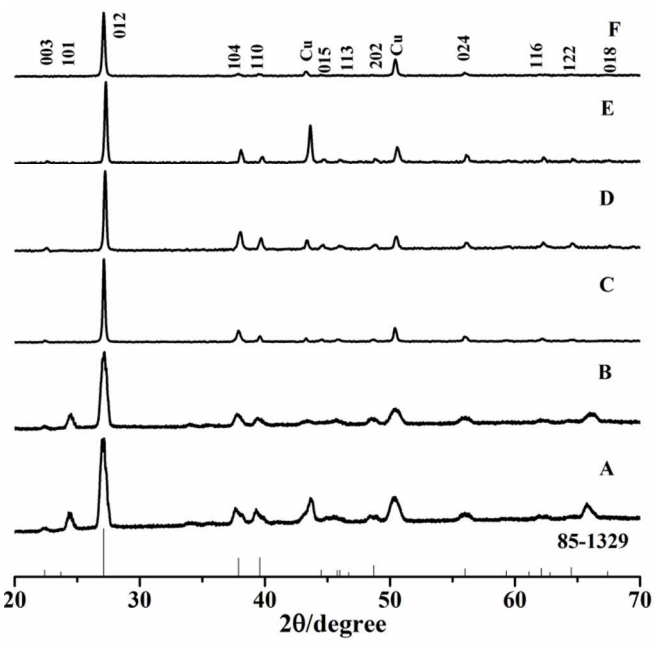

Figure 5. X-ray diffraction patterns of electrodeposited bismuth presence/absence of additives (Table 1 - Samples A-F)

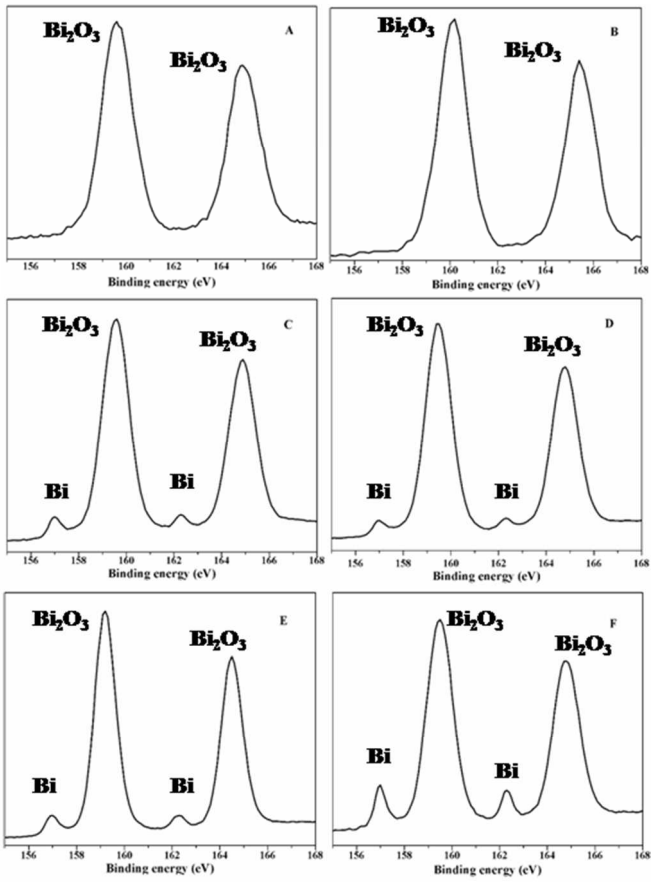

Figure 6. XPS spectra of electrodeposited bismuth $Bi4f_{7/2}$, $Bi4f_{5/2}$ spectra in presence/absence of additives (Table 1 - samples A-F)

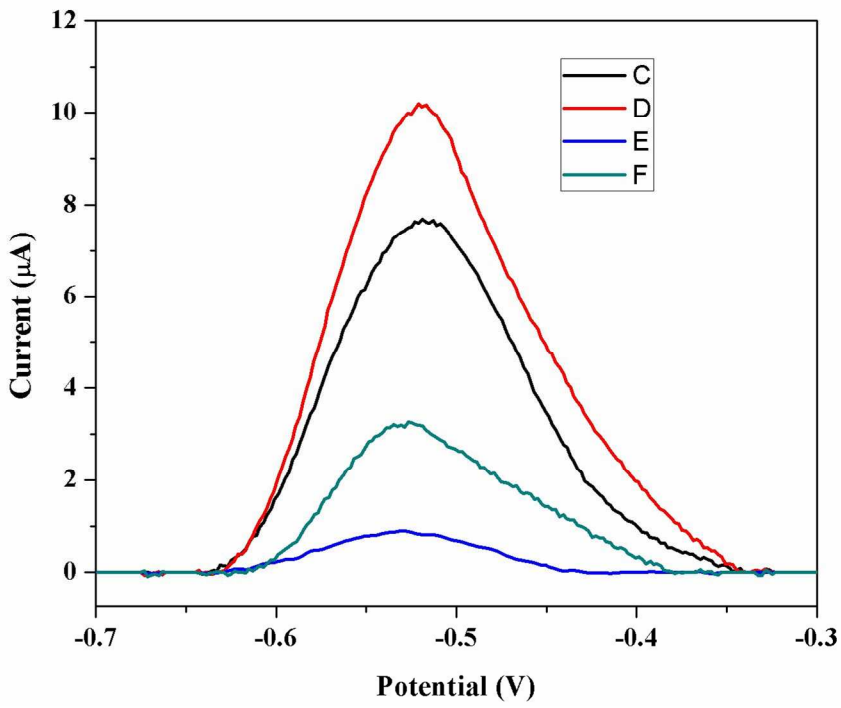

Figure 7. Square wave anodic stripping voltammograms of Pb^{2+} at 50 ppb on bismuth modified electrodes. Sample codes correspond to those used in Table 1.

Table 1. Electrodeposition of bismuth on polycrystalline copper electrodes: Systems studied and morphologies obtained.

Sample	**Bi^{3+} (mM)**	**HNO_3 (M)**	**Additives**	**Current Density (mA/cm^2)**	**Morphology Observed**
A	10	0.4	None	10	Hexagonal rods
B	10	0.4	0.1 M CA	10	Flower-like crystallites and cracked fine grains
C	10	0.4	0.1 M CA, 5 gpl PVA	10	Fine, cauliflower-like crystallites
D	10	0.4	0.1 M CA, 5 gpl PVA, 0.01 M BET	10	Smoother grains
E	10	0.4	None	10 (Ton = 10 ms Toff = 10 ms)	Spindle-like crystallites
F	10	0.4	0.1 M CA, 5 gpl PVA, 0.01 M BET	10 (Ton = 10 ms Toff = 10 ms)	Sea urchin-like crystallites

ASSOCIATED CONTENT

Supporting Information. Figures containing (1) Structure of the additives, (2) Rotating disk voltammograms for bismuth deposition from baths containing additives, (3) Cyclic voltammograms for bismuth deposition, (4) Photographs of electrodeposited bismuth films, (5) Scanning electron microscope images, and (6) X-ray photoelectron spectra of bismuth thin films; The supporting information is available free of charge via the Internet at http://pubs.acs.org.

AUTHOR INFORMATION

Corresponding Author

Murali Rangarajan

Center of Excellence in Advanced Materials and Green Technologies, Department of Chemical Engineering and Materials Science, Amrita School of Engineering Coimbatore, Amrita Vishwa Vidyapeetham, Amrita University, Coimbatore, INDIA

Ph: +91-422-268-5564, Fax: +91-422-265-6274

E-mail: r_murali@cb.amrita.edu

ACKNOWLEDGMENT

Amrita University researchers acknowledge the financial support of Defence Research and Development Organization, New Delhi, India, and the infrastructure provided by Amrita University. GO-I thanks to Portuguese Foundation for Science and Technology (FCT - SFRH/BPD/90562/2012). TEMA/DEM researchers also acknowledge FCT grant UID/EMS/00481/2013. S. J. acknowledges that the ASTUTE 2020 (Advanced Sustainable

Manufacturing Technologies; Project number: 80814) operation has been part-funded by the European Regional Development Fund through the Welsh Government and the participating Higher Education Institutions.

REFERENCES

1. Healy, J. P.; Pletcher, D.; Goodenough, M. The Chemistry of the Additives in an Acid Copper Electroplating Bath. Part I. Polyethylene Glycol and Chloride Ion. *J. Electroanal. Chem*. **1992**, *338*, 155-165.

2. Popescu, A.; Woods, L. M. Valleytronics, Carrier Filtering and Thermoelectricity in Bismuth: Magnetic Field Polarization Effects. *Adv. Funct. Mater*. **2012**, *22*, 3945-3949.

3. Garcia, N.; Kao, Y. H.; Strongin, M. Galvanomagnetic Studies of Bismuth Films in the Quantum-Size-Effect Region. *Phys. Rev. B* **1972**, *5*, 2029-2039.

4. Son, J. S.; Park, K.; Han, M.-K.; Kang, C.; Park, S.-G.; Kim, J.-H.; Kim, W.; Kim, S.-J.; Hyeon, T. Large-Scale Synthesis and Characterization of the Size-Dependent Thermoelectric Properties of Uniformly Sized Bismuth Nanocrystals. *Angew. Chem*. **2011**, *123*, 1399-1402.

5. Yang, F. Y.; Liu, K.; Hong, K. M.; Reich, D. H.; Searson, P. C.; Chien, C. L. Large Magnetoresistance of Electrodeposited Single-Crystal Bismuth Thin Films. *Science* **1999**, *284*, 1335-1337.

6. O'Brien, B.; Plaza, M.; Zhu, L. Y.; Perez, L.; Chien, C. L.; Searson, P. C. Magnetotransport Properties of Electrodeposited Bismuth Films. *J. Phys. Chem. C* **2008**, *112*, 12018-12023.

7. Imamura, A.; Kimura, M.; Kon, T.; Sunohara, S.; Kobayashi, N. Bi-Based Electrochromic Cell with Mediator for White/Black Imaging. *Sol. Energ. Mater. Sol. Cells* **2009**, *93*, 2079-2082.

8. Svancara, I.; Prior, C.; Hocevar, S. B.; Wang J. A Decade with Bismuth-Based Electrodes in Electroanalysis. *Electroanalysis* **2010**, *22*, 1405-1420.

9. Som, T.; Simo, A.; Fenger, R.; Troppenz, G. V.; Bansen, R.; Pfänder, N.; Emmerling, F.; Rappich, J.; Boeck, T.; Rademann, K. Bismuth Hexagons: Facile Mass Synthesis, Stability and Applications. *ChemPhysChem* **2012**, *13*, 2162-2169.

10. Wang, J.; Wang, X.; Peng, Q.; Li, Y. Synthesis and Characterization of Bismuth Single-Crystalline Nanowires and Nanospheres. *Inorg. Chem*. **2004**, *43*, 7552-7556.

11. Yang, M. Fern-Shaped Bismuth Dendrites Electrodeposited at Hydrogen Evolution Potentials. *J. Mater. Chem*. **2011**, *21*, 3119-3124.

12. Wang, W. Z.; Poudel, B.; Ma, Y.; Ren, Z. F. Shape Control of Single Crystalline Bismuth Nanostructures. *J. Phys. Chem. B* **2006**, *110*, 25702-25706.

13. Boldt, R.; Kaiser, M.; Köhler, D.; Krumeich, F.; Ruck, M. High-Yield Synthesis and Structure of Double-Walled Bismuth-Nanotubes. *Nano Lett*. **2010**, *10*, 208-210.

14. Fu, R.; Xu, S.; Lu, Y.-N.; Zhu, J.-J. Synthesis and Characterization of Triangular Bismuth Nanoplates. *Cryst. Growth Des*. **2005**, *5*, 1379-1385.

15. Ni, Y.; Zhang, Y.; Zhang, L.; Hong, J. Mass Synthesis of Dendritic Bi Nanostructures by a Facile Electrodeposition Route and Influencing Factors. *CrystEngComm* **2011**, *13*, 794-799.

16. Derrouiche, S.; Loebick, C. Z.; Pfefferle, L. Optimization of Routes for the Synthesis of Bismuth Nanotubes: Implications for Nanostructure Form and Selectivity. *J. Phys. Chem. C* **2010**, *114*, 3431-3440.

17. Rajamani, A. R.; Ragula, U. B. R.; Kothurkar, N.; Rangarajan, M. Nano- and Micro-Hexagons of Bismuth on Polycrystalline Copper: Electrodeposition and Heavy Metal Sensing. *CrystEngComm* **2014**, *16*, 2032-2038.

18. Das, A.; Sangaranarayanan, M. V. Shape-Controlled Synthesis of Three-Dimensional Triangular Bismuth Microstructures and Sensing of H_2O_2. *CrystEngComm* **2016**, *18*, 1147-1155.

19. Tsai, Y.-D.; Lien, C.-H.; Hu, C.-C. Effects of Polyethylene Glycol and Gelatin on the Crystal Size, Morphology, and Sn^{2+}-Sensing Ability of Bismuth Deposits. *Electrochim. Acta* **2011**, *56*, 7615-7621.

20. Yang, M. L.; Hu, Z. B. Electrodeposition of Bismuth onto Glassy Carbon Electrodes from Nitrate Solutions. *J. Electroanal. Chem*. **2005**, *583*, 46-55.

21. Hara, M.; Nagahara, Y.; Inukai, J.; Yoshimoto, S.; Itaya, K. In Situ STM Study of Underpotential Deposition of Bismuth on Au(1 1 0) in Perchloric Acid Solution. *Electrochim. Acta* **2006**, *51*, 2327-2332.

22. Liu, Z.; Zein El Abedin, S.; Borisenko, N.; Endres, F. Influence of an Additive on Zinc Electrodeposition in the Ionic Liquid 1-Ethyl-3-methylimidazolium Trifluoromethylsulfonate. *ChemElectroChem* **2015**, *2*, 1159-1163.

23. Zarkadas, G. M.; Stergiou, A.; Papanastasiou, G. Influence of Citric Acid on the Silver Electrodeposition from Aqueous $AgNO_3$ Solutions. *Electrochim. Acta* **2005**, *50*, 5022-5031.

24. Kim, M. J.; Choe, S.; Kim, H. C.; Cho, S. K.; Kim, S.-K.; Kim, J. J. Electrochemical Behavior of Citric Acid and Its Influence on Cu Electrodeposition for Damascene Metallization. *J. Electrochem. Soc*. **2015**, *162*, D354-D359.

25. Wang, T.; Chen, Y.-N.; Chiang, C.-C.; Hsieh, Y.-K.; Li, P.-C.; Wang, C.-F. Carbon-Coated Hematite Electrodes with Enhanced Photoelectrochemical Performance Obtained through an Electrodeposition Method with a Citric Acid Additive. *ChemElectroChem* **2016**, *3*, 1-11.

26. Tsai, Y.-D.; Hu, C.-C. Composition Control of Sn–Bi Deposits: Interactive Effects of Citric Acid, Ethylenediaminetetraacetic Acid, and Poly(ethylene glycol). *J. Electrochem. Soc*. **2009**, *156*, D490-D496.

27. Tsai, Y.-D.; Hu, C.-C. Composition Control of Lead-Free Sn–Bi Deposits Using Experimental Strategies. *J. Electrochem. Soc*. **2009**, *156*, D58-D63.

28. Ramezanzadeh, B.; Vakili, H.; Amini, R. The Effects of Addition of Poly(vinyl) Alcohol (PVA) as a Green Corrosion Inhibitor to the Phosphate Conversion Coating on the Anticorrosion and Adhesion Properties of the Epoxy Coating on the Steel Substrate. *Appl. Surf. Sci*. **2015**, *327*, 174-181.

29. Çakir, A.; Ak Azem, F.; Ungan, G. Use of Polyvinyl Alcohol to Improve Adhesion Properties of Hap Coating on Ti–6Al–4V. *J. Biomech*. **2011**, *44*, ee21.

30. Bard, A. J.; Faulkner, L. R. *Electrochemical Methods: Fundamentals and Applications*; 2nd Ed,; John Wiley & Sons, Inc: New York, **2001**.

31. Scharifker, B.; Hills, G. Theoretical and Experimental Studies of Multiple Nucleation. *Electrochim. Acta* **1983**, *28*, 879-889.

32. Asato, E.; Katsura, K.; Mikuriya, M.; Turpeinen, U.; Mutikainen, I.; Reedijk, J. Synthesis, Structure, and Spectroscopic Properties of Bismuth Citrate Compounds and the Bismuth-Containing Ulcer-Healing Agent Colloidal Bismuth Subcitrate (CBS). 4.[1] Crystal

Structure and Solution Behavior of a Unique Dodecanuclear Cluster $(NH_4)_{12}[Bi_{12}O_8(cit)_8](H_2O)_{10}$. *Inorg. Chem*. **1995**, *34*, 2447-2454.

33. Hope, G. A.; Brown, G. M. A Study of the Adsorption of Polymeric Additives at a Copper Electrode and their Incorporation into Copper Deposits by Electrodeposition. In Proceedings of the Sixth International Symposium on Electrode Processes, Wieckowski, A.; Itaya, K., Ed. *Electrochem. Soc*.; Los Angeles, CA, **1996**, *96*, 215-222.

34. Masood, S.; Perveen, R.; Ashfaq, M. Copper Fractal Growth Pattern in Polymer Systems. *Int. J. Chem*. **2012**, *4*, 15-21.

35. Chandrasekar, M. S.; Pushpavanam, M. Pulse and Pulse Reverse Plating-Conceptual, Advantages and Applications. *Electrochim. Acta* **2008**, *53*, 3313-3322.

36. Cao, L.; Lu, X.; Pu, F.; Yin, X.; Xia, Y.; Huang, W.; Li, Z. Facile Fabrication of Superhydrophobic Bi/Bi_2O_3 Surfaces with Hierarchical Micro-Nanostructures by Electroless Deposition or Electrodeposition. *Appl. Surf. Sci*. **2014**, *288*, 558-563.

37. Rehacek, V.; Hotovy, I.; Vojs, M.; Mika, F. Bismuth Film Electrodes for Heavy Metals Determination. *Microsys. Technol*. **2008**, *14*, 491-498.

38. Arduini, F.; Calvo, J. Q.; Palleschi, G.; Moscone, D.; Amine, A. Bismuth-Modified Electrodes for Lead Detection. *TrAC Trends Anal. Chem*. **2010**, *29*, 1295-1304.

39. March, G.; Nguyen, T.; Piro, B. Modified Electrodes Used for Electrochemical Detection of Metal Ions in Environmental Analysis. *Biosensors* **2015**, *5*, 241-275.

40. Farghaly, O. A.; Ghandour, M. A. Square-Wave Stripping Voltammetry for Direct Determination of Eight Heavy Metals in Soil and Indoor-Airborne Particulate Matter. *Environ. Res.* **2005**, *97,* 229-35.

GRAPHICAL ABSTRACT